Eleventh International Conference on Computational Fluid Dynamics (ICCFD11), Maui, HI, July 11-15, 2022

ICCFD11-2022-3203

Characterization and Modeling of Spallation in Thermal Protection Systems

K. Price*, S. Bailey* and A. Martin*
Corresponding author: kristen.price@uky.edu

* Mechanical Engineering, University of Kentucky, Lexington, KY 40506, USA.

Abstract: The spallation of particles resulting from the breaking of individual carbon fibers within TPS material results in additional mass loss and reduces TPS efficiency. Understanding this process is crucial to more accurately modeling these TPS, both in the response of the material and the effects on the surrounding flow. Analysis of arc-jet tests investigating these spalled particles have provided insight into their production, size, and quantities. Modeling of samples for additional testing to further investigate and physically capture these spalled particles is provided in this work. This will allow for validation of previous analysis and help in building a more autonomous model of the spallation process.

Keywords: Thermal Protection Systems, Spallation, Arc-Jets, Ablation Modeling, Computational Fluid Dynamics.

1 Introduction

During atmospheric entry, a thermal protection system (TPS) is used to protect space vehicles from the large amounts of heat incurred when drag forces are used to slow down the vehicle. These TPS are often made of ablative materials, which typically consist of a carbon fiber matrix impregnated with a polymer resin, making the material very porous and lightweight. For example, Phenolic Impregnated Carbon Ablator (PICA) is an ablative material made from the carbon fiber preform known as FiberForm®. The ablation process burns up the material so that the heat is absorbed through mass removal instead of conduction through the vehicle. The fibrous nature of these TPS, however, results in a very brittle material that is further worn away by mechanical erosion and oxidation. The process of spallation occurs when pieces of this material break off and are ejected into the flow. This increases recession rates and therefore must be accounted for in modeling and design.

The process of spallation is currently modeled using an empirical rate in which it is modeled as a percentage of the ablation rate, often 5% for PICA [1, 2]. However, understanding the number and size of particles produced can help to refine this number and more accurately model the amount of mass loss occurring. This was explored in previous arc-jet testing conducted at the Hypersonic Materials Environmental Test System (HyMETS) arc-jet facility at NASA Langley Research Center [3], and plans are underway for an additional arc-jet campaign in order to validate previous analysis. The following work is in preparation for this additional arc-jet campaign, the goal of which is to physically capture spalled particles for direct measurement and analysis.

2 Background

The Kentucky Aerothermodynamics and Thermal-response System (KATS) solver has a computational fluid dynamics (CFD) module that can model the flow surrounding a vehicle or material sample [4, 5, 6, 7]. A Lagrangian particle code that is one-way coupled to a CFD solution is utilized to model spalled particles ejected from a TPS material and inserted into the surrounding flow, provided an initial particle position,

velocity, and size [8, 9, 10]. This code is capable of recreating trajectories measured in previous experiments, as discussed in Davuluri et al. [11].

Analysis from previous arc-jet campaigns at HyMETS resulted in estimates of particle size, an example distribution of which is given in Figure 1 [12, 13, 14]. Particle trajectories were determined using particle tracking velocimetry with high-speed images captured during testing. From these trajectories, a particle acceleration equation was determined by using Stokes' equation for drag coefficient in a force balance. This was then fit to the velocity versus time of individual particles to estimate the hydraulic diameters given in the probability density function (PDF) shown in Figure 1. By integrating this distribution, a cumulative distribution function (CDF) is determined. This CDF can be used to associate randomly selected numbers between 0 and 1 to an actual particle size, in order to randomly recreate the PDF. Integrating this method into the spallation code allows for randomly modeled particles that statistically represent the particles previously seen in testing.

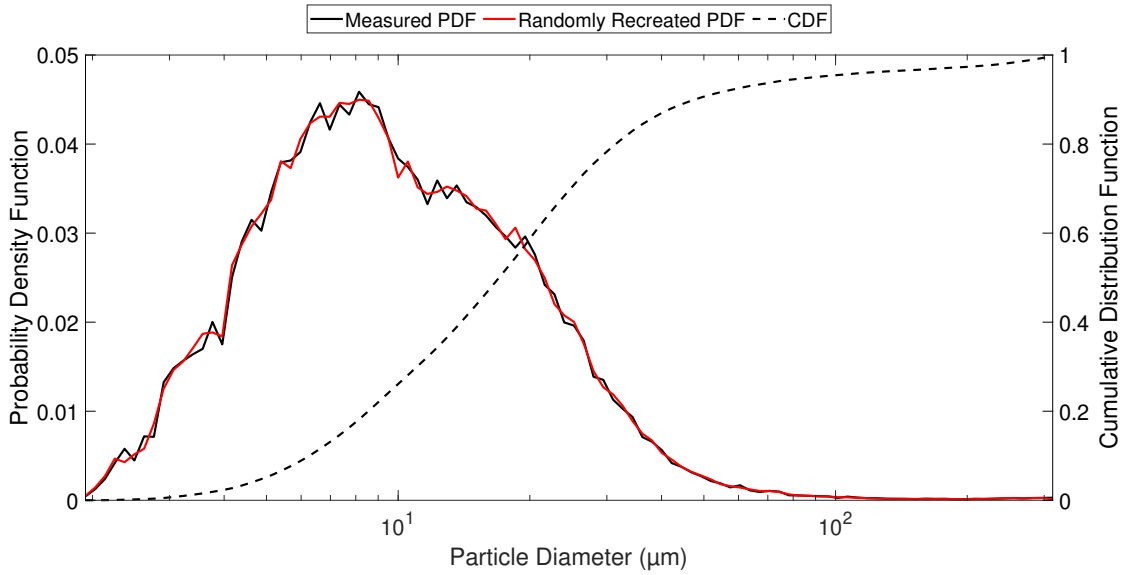

Figure 1: Distribution of spallation particle size, including PDF measured from previous arc-jet campaign, CDF found by integrating PDF, and randomly recreated PDF calculated using the CDF.

Therefore, the spallation code can be used to model various sample geometries proposed for arc-jet testing to determine which will most likely achieve the testing goals. Since the goal of future arc-jet testing is to physically capture spalled particles, various materials were proposed in which particles would embed themselves for later analysis. The most promising material for capturing particles and survive arc-jet conditions is a heat barrier spray known as Cool Gel®. To utilize this gel material, the geometries shown in Figure 2 were designed and analyzed. The proposed samples consist of wedge TPS samples, made of both FiberForm and PICA, held by graphite holders that also contain the gel material. This work will be utilized to model and analyze the various holder geometries and investigate their behavior in the arc-jet.

3 Flow Solutions

The CFD flow solutions found using KATS for these various sample holder geometries assumed flow conditions based on what had been measured in previous HyMETS testing. However, since these conditions were measured in the arc chamber, the flow solution had to be determined in two parts. The arc chamber conditions were used as the inlet values to model the flow in the converging-diverging nozzle portion of the facility. Then, the outlet values from this nozzle solution were used as the inlet values for the test chamber where the sample is.

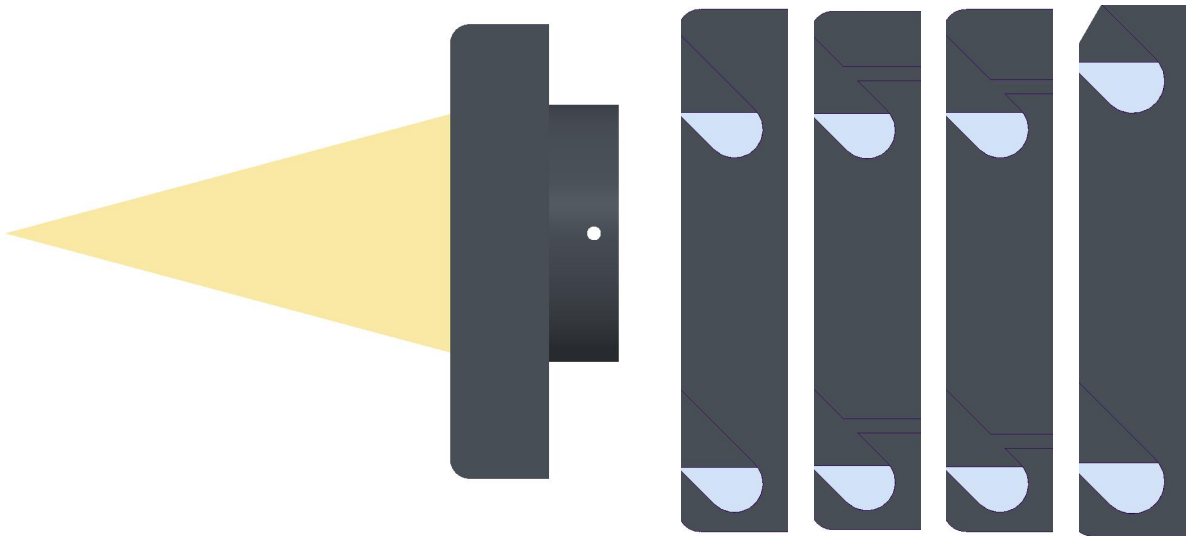

(a) Sample Geometry (b) Original (c) Slot (d) Low Slot (e) Angled

Figure 2: Sample geometry and proposed sample holders. The TPS material is shown in yellow, the graphite holder in black, and the gel material in blue.

The arc chamber conditions, including flow composition, pressure, and enthalpy, that were measured during testing are given in Table 1.

Table 1: Table of HyMETS test flow conditions.

Gas	Ar Flow (slpm)	N_2 Flow (slpm)	O_2 Flow (slpm)	Pressure (kPa)	Bulk Enthalpy (MJ/kg)
Air	22	337	90	137	11.0

From these measurements, the elemental composition of the flow must be calculated in order to utilize an equilibrium solver to calculate the remaining flow conditions. First, the mole fraction, χ_s, of each species was calculated from the volumetric flow rates, $\dot{V}$, using

$$\chi_s = \frac{\dot{V}_{s,slpm}}{\sum \dot{V}_{s,slpm}} \tag{1}$$

where the flow rate is in standard liters per minute. This results in $\chi_{Ar} = 5\%$, $\chi_{N2} = 75\%$, and $\chi_{O2} = 20\%$ for the conditions given in Table 1.

Next, the elemental composition, e_i, can be calculated using

$$e_i = \frac{n_i \chi_s}{\sum n_i \chi_s} \tag{2}$$

where n_i is the number of atoms of each element in a species. This results in $e_{Ar} = 0.0256$, $e_N = 0.7692$, and $e_O = 0.2051$ for the flow conditions given here. These values can then be utilized as the flow mixture in the equilibrium solver Mutation++, which can be used to calculate the remaining flow conditions modeled at the inlet [15].

Utilizing the pressure given in Table 1, various temperatures can be tried until the enthalpy output in Mutation++ matches that also given in the table. Additionally, at this temperature and pressure, the species density values can also be calculated using Mutation++. Assuming these values to be that of the nozzle inlet, the inlet velocity, U, can also be calculated using

$$U = \frac{\sum \dot{m}_{s,kg/s}}{A_{in}\rho_{tot}} \tag{3}$$

where ρ_{tot} is the sum of the species density values and A_{in} is the cross-sectional area of the nozzle inlet (radius ∼11.11 mm). The mass flow rate, $\dot{m}$, of each species calculated in kg/s can be found from

$$\dot{m}_{s,g/s} = \dot{V}_{s,slpm} \times \frac{P_{std}}{T_{std}} \times \frac{1}{R_s} \times \frac{1\text{min}}{60\text{s}} \times \frac{0.001\text{m}^3}{1\text{L}} \tag{4}$$

where T_{std} and P_{std} are the standard temperature and pressure, respectively, and R_c is the specific gas constant of the species. These are found to be $\dot{m}_{\text{Ar}} = 0.65$ g/s, $\dot{m}_{\text{N}_2} = 7.02$ g/s, and $\dot{m}_{\text{O}_2} = 2.14$ g/s.

Thus, all of these values are utilized as the nozzle inlet and initial conditions, as given in Table 2. The nozzle wall temperature is assumed to be a cold-wall condition at 350K, and the nozzle outlet pressure assumes the vacuum pressure of 228 Pa [16].

Table 2: Table of inlet and initial conditions for nozzle solution.

Temperature (K)	Partial Densities (kg/m^3)	Velocity (m/s)
5510	Ar : 4.86005×10^{-3}	353
	N_2 : 4.78602×10^{-2}	
	O_2 : 7.32008×10^{-5}	
	NO : 1.13608×10^{-3}	
	N : 2.75547×10^{-3}	
	O : 1.48974×10^{-2}	

The nozzle mesh assumes axi-symmetry and is given in Figure 3(a). The corresponding Mach number solution calculated using the inputs given in Table 2 and the chemical reactions for 5-species air is given in Figure 3(b).

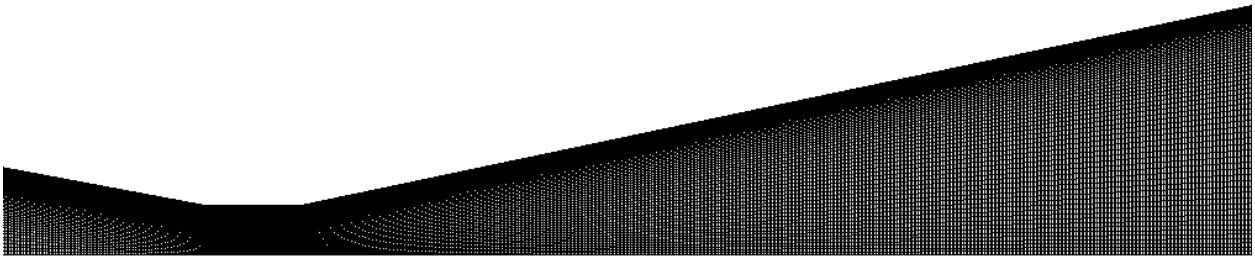

(a) Nozzle Mesh

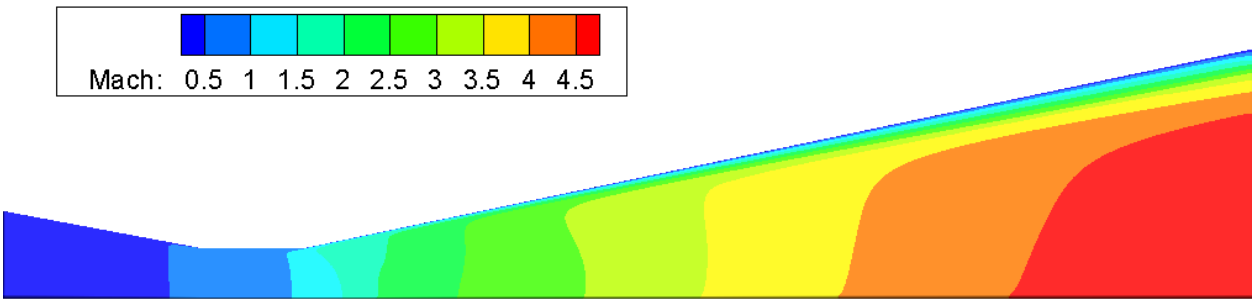

(b) Nozzle Solution

Figure 3: Nozzle mesh and corresponding Mach number solution.

The values at the nozzle exit centerline were then utilized as the inlet conditions for the sample solutions. These were determined directly from the CFD results and are given in Table 3. Note that the y-component of velocity is left at zero due to a one-dimensional velocity assumption. Both the translational-rotational and vibrational-electronic wall temperatures for the sample are set at the average surface temperature measured by a pyrometer during experiments, which was found to be 2125.51 K.

Table 3: Table of input conditions for sample solutions.

Translational-Rotational Temperature (K)	Vibrational-Electronic Temperature (K)	Partial Densities (kg/m^3)	Velocity (m/s)
887.79	4976.83	Ar : 6.202×10^{-5}	3390.43
		N_2 : 6.358×10^{-4}	
		O_2 : 3.550×10^{-7}	
		NO : 7.131×10^{-9}	
		N : 1.690×10^{-5}	
		O : 1.984×10^{-4}	

The sample meshes, given in Figures 4(a)-4(d), are symmetrical, so only the top half of each is modeled. Note that, although the samples begin as pointed wedges, they are modeled here with rounded tips in order to mimic the mid-test recession seen in previous analysis. Figures 4(e)-4(h) show the resulting sample Mach number solutions, with streamlines included.

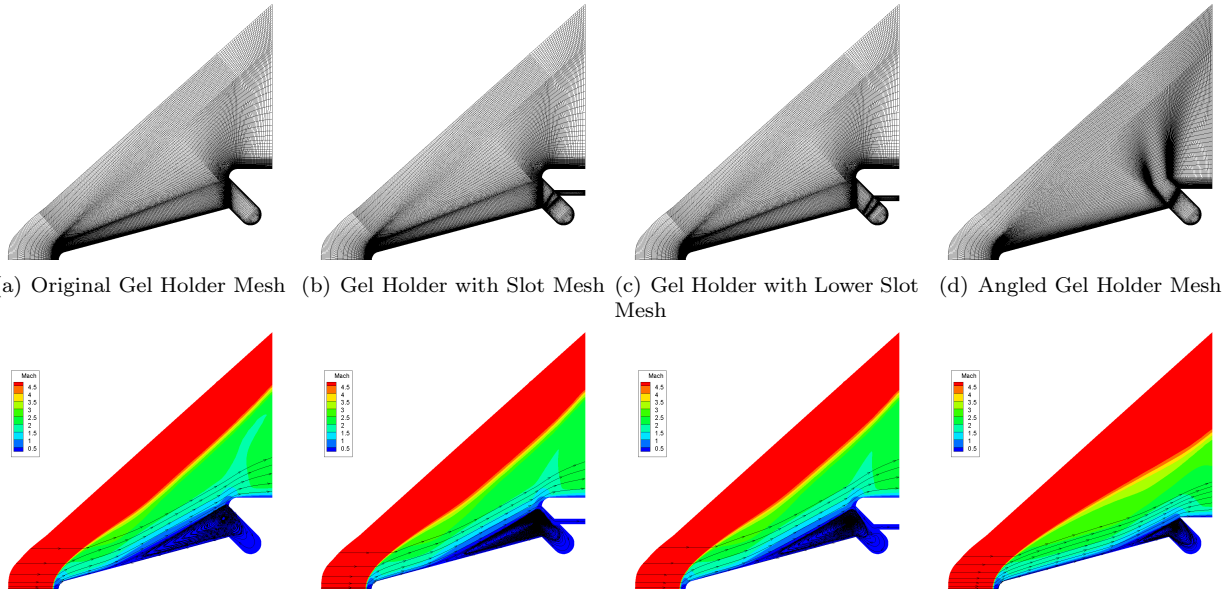

(a) Original Gel Holder Mesh (b) Gel Holder with Slot Mesh (c) Gel Holder with Lower Slot Mesh (d) Angled Gel Holder Mesh

(e) Original Gel Holder Solution (f) Gel Holder with Slot Solution (g) Gel Holder with Lower Slot Solution (h) Angled Gel Holder Solution

Figure 4: Sample meshes and corresponding Mach number solutions with streamlines.

As seen in Figure 4, a recirculation zone builds up in front of the part of the sample holders that are normal to the flow, which could prevent particles from being captured. After initially seeing this in Figure 4(e), the holder geometries in Figures 2(c) and 2(d) were designed with an additional slot in order to relieve the pressure and reduce this recirulation zone. Similarly, the geometry in Figure 2(e) minimizes the amount of material normal to the flow to decrease the recirculation zone. However, in order to determine which of these geometries will be most effective for particle capture, the actual particle trajectories will be modeled.

4 Spallation Particles

The spallation model utilizes a Lagrangian particle code one-way coupled with a CFD solution to model particles injected into a flow field. A set of 100 particles with diameters matching the distribution given in Figure 1 were modeled randomly all along the TPS wedge with negligible initial velocities tangent to the sample surface. The results of this analysis are shown in Figure 5.

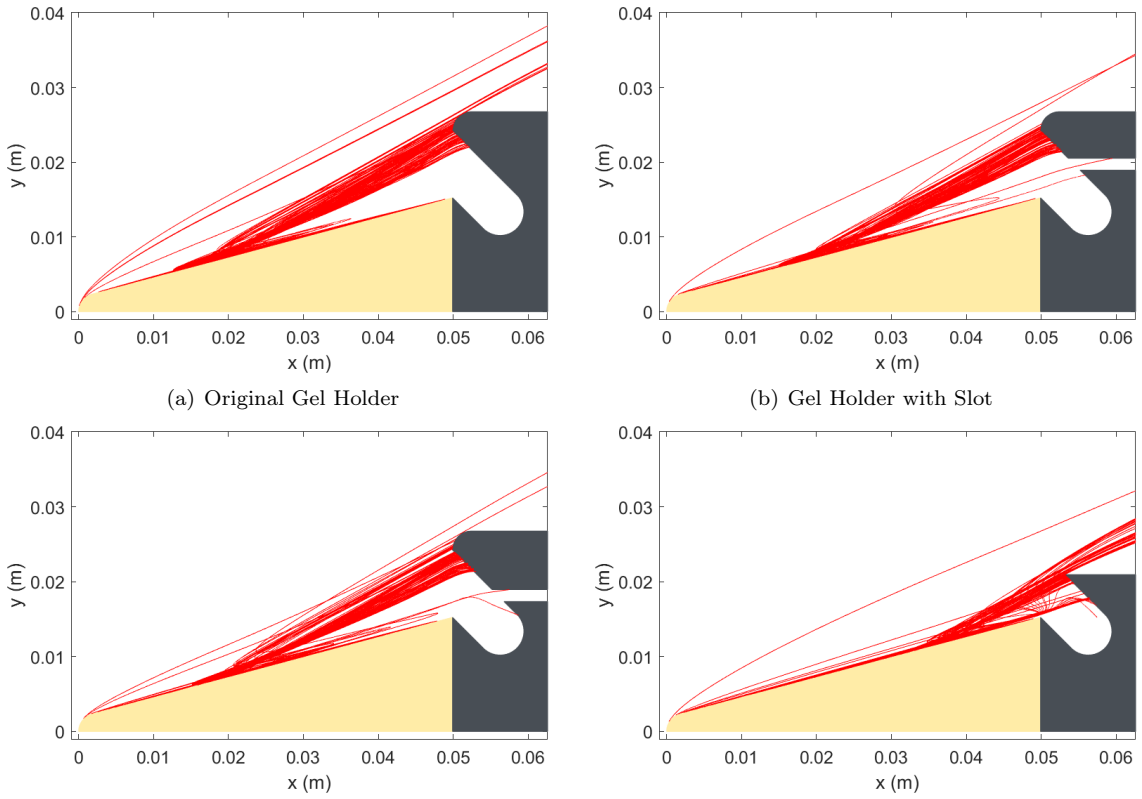

(a) Original Gel Holder

(b) Gel Holder with Slot

(c) Gel Holder with Lower Slot

(d) Angled Gel Holder

Figure 5: Particles modeled for each proposed sample holder geometry using the spallation code.

This figure demonstrates that all of the sample geometries are capable of capturing particles, but table 4 lists what percentage of particles landed within the gel pocket. From this table, it is clear that both the slotted and angled holder geometries increase the ability to capture particles. Although it appears that the slotted holders will be the most effective at capturing particles, a more detailed analysis can help to investigate any bias that may occur in the particles that are being captured.

Table 4: Percentage of particles landing in gel pocket.

Original Gel Holder	Gel Holder with Slot	Gel Holder with Lower Slot	Angled Gel Holder
52%	88%	81%	67%

First, Figure 6 demonstrates particles that have been ejected at every position along the TPS wedge surface. These particles were all modeled as 10 microns in diameter, as this is the most common value given in Figure 1. This analysis is to ensure that particles at and around the tip of the wedge are able to be captured, as this is the region of high heating from which most particles will be originating.

As seen in Figure 6, none of the particles from the direct tip of the wedge are able to be captured. However, many particles from the surrounding areas, where high heating is still occurring, are hitting most centrally in the gel pockets. Additionally, particles from the angled part of the wedge travel more directly towards the pocket. Although these samples are modeled at the expected mid-test recession, they will begin

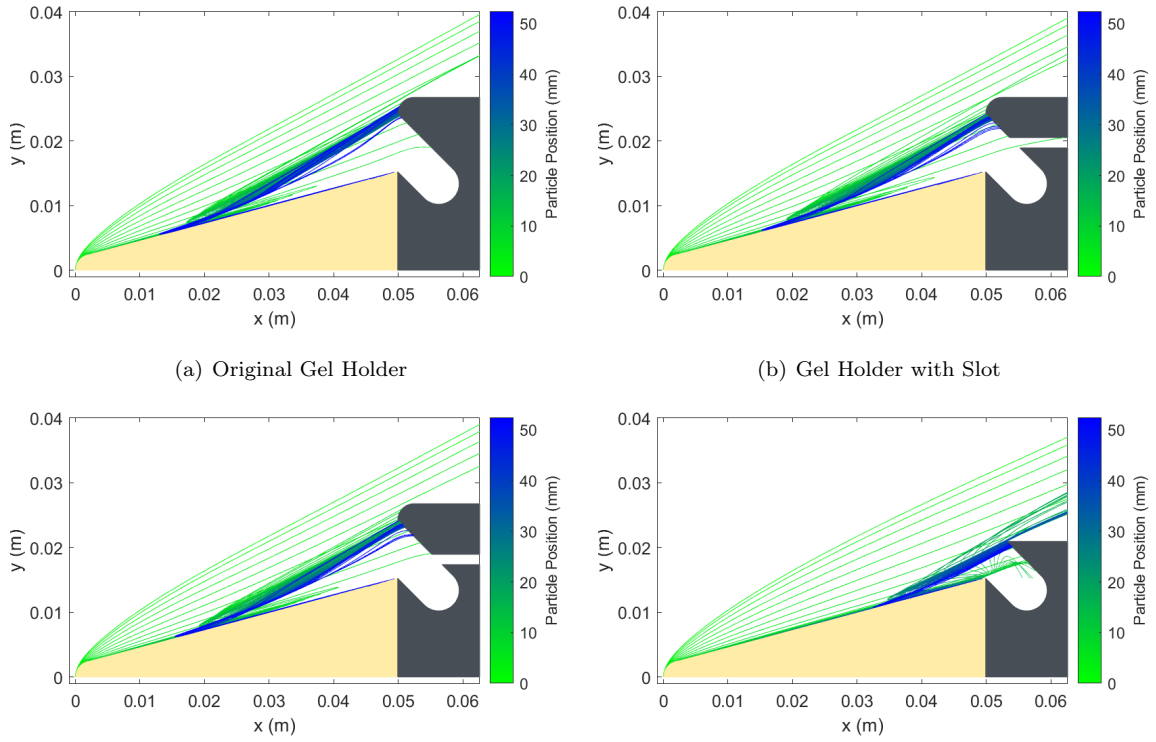

(a) Original Gel Holder

(b) Gel Holder with Slot

(c) Gel Holder with Lower Slot

(d) Angled Gel Holder

Figure 6: 10 μm particles modeled all along sample wedge. Green indicates particles at tip of wedge, while blue indicates particles at the back of wedge, near particle capture material.

as pointed wedges, at which point particles from the direct tip are more likely to be captured before the sample begins to change shape.

In comparing these geometries, Figures 6(b) and 6(c) demonstrate that the slots relieve the pressure enough to bring a significant amount of particles inside the gel pocket. However, the geometry in Figure 6(d) allows a greater range of particles to hit centrally in the pocket. Therefore, the angled gel holder is best suited to capturing particles from the widest range of ejection locations.

Similarly, Figure 7 demonstrates the results of ejecting particles with the range of sizes given in Figure 1. All of these particles are ejected from the same location at the edge of the rounded tip of the nozzle, as this is still within the region of high-heating, but along the angled portion of the wedge, where trajectories are more likely to travel directly towards the pocket.

Figures 7(a)-7(c) show that not a lot of particles from this position are likely to be captured, but small particles are more likely to be captured than larger ones. This result, along with the many 10 micron particles from other locations that were able to be captured as discussed for Figure 6, confirms that the expected particle sizes can be captured from the expected particle ejection locations, as the previously measured particle distributions are largely leaning towards smaller particles. However, the angled gel holder is once again better at capturing the entire range of particle sizes. Although a few smaller particles are not able to captured, the entire rest of the range hits centrally in the gel pocket.

Therefore, although the random particle models demonstrated that the slotted holders were most effective for particle capture, the angled holders may be better suited for the specific range of particle sizes and ejection locations expected for this testing.

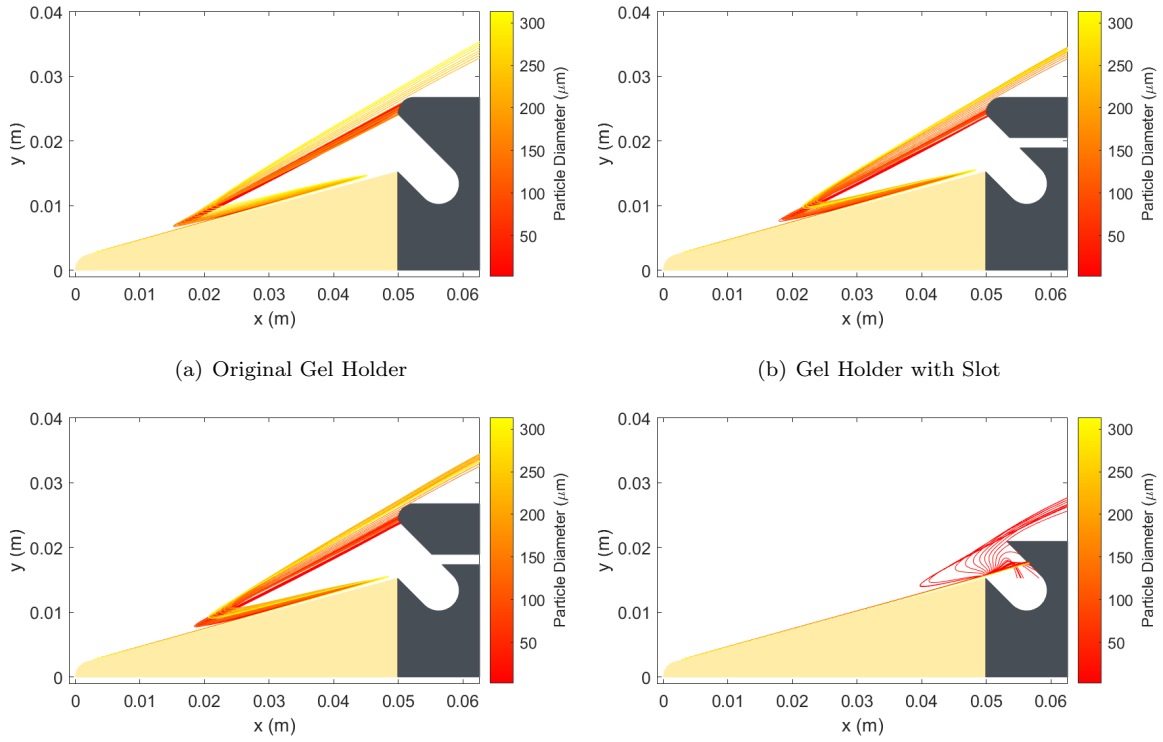

(a) Original Gel Holder

(b) Gel Holder with Slot

(c) Gel Holder with Lower Slot

(d) Angled Gel Holder

Figure 7: Particles modeled for each proposed sample holder geometry using entire range of particle size distribution near tip of wedge. Red indicates smaller particles, while yellow indicates larger particles.

5 Conclusions

In preparation for an additional arc-jet campaign to capture particles and validate previous analysis of particle size, multiple sample geometries were modeled with CFD and a spallation code. In comparing the various geometries, the slotted gel holders proved most effective for the overall random model, but the angled geometry was better fit for the targeted particles. However, additional analysis involving specific arc-jet conditions and manufacturability of the various samples may provide further insight into which will be best suited for additional testing.

6 Acknowledgements

Financial support for this work was provided by NASA Space Tech-REDDI-2021 NSTGRO award no. 80NSCC21K1255, as well as by NASA Kentucky EPSCoR Award no. 80NSSC20M0047. The authors would also like to thank the University of Kentucky Center for Computational Sciences and Information Technology Services Research Computing for their support and use of the Lipscomb Compute Cluster and associated research computing resources.

References

[1] F.S. Milos and Y.-K. Chen. Ablation, thermal response, and chemistry program for analysis of thermal protection systems. *Journal of Spacecraft and Rockets*, 50(1), January–February 2013.

[2] Frank S. Milos, Matthew J. Gasch, and Dinesh K. Prabhu. Conformal phenolic impregnated car-

bon ablator (c-pica) arcjet testing, ablation and thermal response. *Journal of Spacecraft and Rockets*, 52(3):804–812, 2015.

[3] A. J. Brune, III Bruce, W. E., D. E. Glass, and S. C. Splinter. Computational simulations of the nasa langley hymets arc-jet facility. In *JANNAF - Interagency Propulsion Committee meeting*, page 16, Newport News, VA, United States, December 2017.

[4] R. Fu, H. Weng, J. F. Wenk, and A. Martin. Thermomechanical coupling for charring ablators. *Journal of Thermophysics and Heat Transfer*, 32(2):369–379, 2018.

[5] H. Weng and A. Martin. Multidimensional modeling of pyrolysis gas transport inside charring ablative materials. *Journal of Thermophysics and Heat Transfer*, 28(4):583–597, 2014.

[6] H. Zhang, H. Weng, and A. Martin. *Simulation of Flow-tube Oxidation on the Carbon Preform of PICA*.

[7] U. Duzel, O. Schroeder, and A. Martin. *Computational Prediction of NASA Langley HYMETS Arc Jet Flow with KATS*.

[8] A. Martin, S. C. C. Bailey, F. Panerai, R. S. C. Davuluri, H. Zhang, A. R. Vazsonyi, Z. S. Lippay, N. N. Mansour, J. A. Inman, B. F. Bathel, S. C. Splinter, and P. M. Danehy. Numerical and experimental analysis of spallation phenomena. *CEAS Space Journal*, 8:229–236, 2016.

[9] R. S. C. Davuluri, S. C. C. Bailey, K. A. Tagavi, and A. Martin. A drag coefficient model for lagrangian particle dynamics relevant to high-speed flows. *International Journal of Heat and Fluid Flow*, 87:108706, 2021.

[10] R. S. C. Davuluri, H. Zhang, and A. Martin. Numerical study of spallation phenomenon in an arc-jet environment. *Journal of Thermophysics and Heat Transfer*, 30(1):32–41, 2016.

[11] R. Davuluri, S. C. C. Bailey, K. Tagavi, and A. Martin. Numerical reconstruction of spalled particle trajectories in an arc-jet environment. In *AIAA SciTech 2021 Forum*, AIAA 2021-1172, Virtual, January 2021.

[12] K. J. Price, J. M. Hardy, C. G. Borchetta, F. Panerai, S. C. C. Bailey, and A. Martin. Analysis of spallation products using arc-jet experiments. In *AIAA Scitech 2020 Forum*, AIAA 2020-1707, Orlando, Florida, January 2020.

[13] K. J. Price, J. M. Hardy, C. G. Borchetta, F. Panerai, S. C. C. Bailey, and A. Martin. Spallation particle size analysis resulting from arc-jet experiments. In *AIAA Aviation 2020 Forum*, AIAA 2020-3279, Virtual, June 2020.

[14] K. J. Price, F. Panerai, C. G. Borchetta, J. M. Hardy, A. Martin, and S. C. C. Bailey. Arc-jet measurements of low-density ablator spallation. *Experimental Thermal and Fluid Science*, 133:110544, 2022.

[15] James B. Scoggins, Vincent Leroy, Georgios Bellas-Chatzigeorgis, Bruno Dias, and Thierry E. Magin. Mutation++: Multicomponent thermodynamic and transport properties for ionized gases in c++. *SoftwareX*, 12:100575, 2020.

[16] Umran Duzel, Olivia Schroeder, and Alexandre Martin. Computational prediction of NASA langley HYMETS arc jet flow with KATS. In *2018 AIAA Aerospace Sciences Meeting*. American Institute of Aeronautics and Astronautics, January 2018.